Nanoscale

Accepted Manuscript

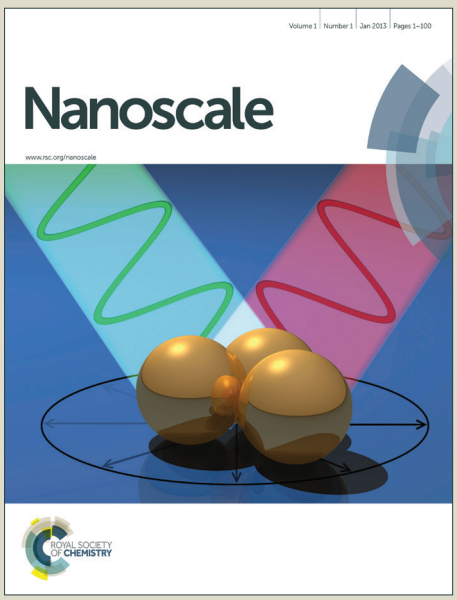

ROYAL SOCIETY OF CHEMISTRY

www.rsc.org/nanoscale

Synthesis and Microwave Absorption Enhancement of graphene@Fe_3O_4@SiO_2@NiO nanosheets hierarchical structures

Lei Wang* Ying Huang[*] Xu Sun Haijian Huang Panbo Liu Meng Zong Yan Wang

Department of Applied Chemistry, school of Science, Northwestern Polytechnical University, Xi'an, P.R China

Key Laboratory of Space Applied Physics and chemistry, Ministry of Education, Northwestern Polytechnical University, Xi'an, P.R China

Abstract

Hierarchical structures of graphene@Fe_3O_4@SiO_2@NiO nanosheets were prepared by combining the versatile sol-gel process with a hydrothermal reaction. Graphene@Fe_3O_4 composites were first synthesized by the reduction reaction between $FeCl_3$ and diethylene glycol (DEG) in the presence of GO. Then, graphene@Fe_3O_4 was coated with SiO_2 to obtain graphene@Fe_3O_4@SiO_2. Finally, NiO nanosheets were grown perpendicularly on the surface of graphene@Fe_3O_4@SiO_2 and graphene@Fe_3O_4@SiO_2@NiO nanosheets hierarchical structures were formed. Moreover, the microwave absorption properties of both graphene@Fe_3O_4 and graphene@Fe_3O_4@SiO_2@NiO nanosheets were investigated between 2-18 GHz microwave frequency bands. The electromagnetic data demonstrates that graphene@Fe_3O_4@SiO_2@NiO nanosheets hierarchical structures exhibit significantly enhanced microwave absorption properties compared with graphene@Fe_3O_4, which probably originate from the unique hierarchical structure with a large surface area and high porosity.

1. Introduction

Electromagnetic (EM) interference problems have emerged due to the increasing usage of electronic devices and communication facilities in industry, commerce and military affairs [1]. A good way to solve this problem is to use microwave absorption materials to attenuate those

[*] corresponding author
E-mail address: yingh@nwpu.edu.cn, Tel.:+86 2988431636, Fax: +86 2988492724

unwanted electromagnetic energies. The idea EM absorbers are required to have wide absorption frequency range, strong absorption properties, low density, good thermal stability, and antioxidant capability [2]. To date, EM absorption properties of various nanostructures have been investigated in order to reach the ideal targets [3-10]. Among these nanostructures, carbon-based composites exhibit good absorption properties.

Graphene, a new class of two-dimensional carbon nanostructure, has attracted much attention for its unique physical, chemical, and mechanical properties [11]. Graphene possesses not only a stable structure but also high specific surface area and excellent electronic conductivity. These properties make graphene very promising as a lightweight EM absorber [12]. However, the high carrier mobility is harmful to its EM absorption in terms of impedance match mechanism. One of the effective ways to solve the problem is to couple graphene with magnetic constituents [13-17]. Qi and co-works fabricated graphene-Fe_3O_4 nanohybrids, the maximum reflection loss of the nanohybrids was up to -40.36 dB with a thickness of 5.0 mm at 7.04 GHz, and the absorption bandwidth with reflection loss less than -10 dB was about 2 GHz [13]. He et.al prepared laminated magnetic graphene, and the maximum reflection loss was -26.4 dB with a thickness of 4.0 mm at 5.3 GHz, and the absorption bandwidth with reflection loss less than -10 dB was 2 GHz [14]. Yang et.al synthesized bowl-like Fe_3O_4 hollow spheres/reduced graphene oxide nanocomposites, the as-synthesized nanocomposites with a coating layer thickness of 2.0 mm exhibited a maximum absorption of -24 dB at 12.9 GHz as well as a bandwidth of 4.9 GHz (from frequency of 10.8-15.7 GHz) corresponding to reflection loss at -10 dB [15]. Ouyang et.al investigated the electromagnetic absorption properties of graphene/Fe_3O_4@Fe/ZnO quaternary nanocomposites, the results showed that the maximum R_L values were lower than -30 dB for the quaternary

nanocomposites with a thickness of 2.5-5 mm and the absorption bandwidth with R_L values less than -20 dB was up to 7.3 GHz (in the frequency range of 5.9-15.2 GHz) [16]. Chen et.al investigated the microwave absorption properties of mono-dispersed RGO-hematite nanocomposites, the results showed that the nanocomposites not only exhibited a larger reflection loss (-78 dB at 15.4 GHz), but also a wider absorption band (less than -10 dB from 11.3 to 18 GHz) [17]. It can be concluded from the above-mentioned research literatures that good EM absorption properties with lightweight and wide absorption frequency band can be realized by reasonable construction of graphene-based naoncomposites. However, these research articles are focusing mostly on the two-dimensional graphene-based nanocomposites, and only a few studies are looking at the graphene-based hierarchical structures. It is well-known that the absorption properties of a material are closely related to the structure of microwave absorber [18]. Recent advances show that excellent microwave absorption properties can be obtained from hierarchical nanostructures with complicated geometrical morphologies [19].

NiO is an important transition-metal oxide that has been extensively studied in the area of supercapacitors because of its large surface area [20]. The large surface area of absorber helps the enhancement of microwave absorption [19]. Herein, the hierarchical structures consisting of graphene, Fe_3O_4@SiO_2 and NiO nanosheet were fabricated via a multi-step route, and the microwave absorption properties were investigated. The results show that the hierarchical structure exhibits enhanced EM absorption in terms of both the maximum reflection loss value and the absorption bandwidth compared with two-dimensional nanocomposites of graphene@Fe_3O_4. The maximum reflection loss value can reach -51.5 dB at 14.6 GHz with a thickness of only 1.8 mm and the bandwidth corresponding to the reflection loss below -10 dB is 5.1 GHz (from 12.4 to

17.5 GHz).

2. Experimental

All of the chemicals and reagents were purchased from Sinopharm Chmical Reagent Co., Ltd, China and used as received. Deionized water was used for all experiments.

2.1 Preparation of graphene@ Fe_3O_4@ SiO_2@NiO nanosheets hierarchical structures

Graphene Oxide (GO) was synthesized using natural graphite flakes according to the literature method [21]. The preparation of graphene@Fe_3O_4 was carried out by the reduction reaction between $FeCl_3$ and diethylene glycol (DEG) in the presence of GO [22]. graphene@Fe_3O_4@ SiO_2@NiO nanosheets hierarchical structures were prepared according to the literature method [23]. Briefly, as-prepared graphene@Fe_3O_4 was dispersed in a mixture of ethanol (40 mL), water (10 mL) and ammonia (1 mL). Then, 0.2 mL of tetraethylorthosilicate (TEOS) was added dropwise, and the reaction was allowed to proceed for 10 h under stirring. The resulting graphene@Fe_3O_4@SiO_2 composites were washed four times with ethanol by magnetic decantation and dispersed in a blue-cap glass bottle containing 40 mL of DI water and ethanol by ultrasonication for 40 min, followed by addition of 2 g of urea under mild stirring. After 5 min, 6 mL of $Ni(NO_3)_2$ (0.1 M) were added dropwise, and the mixture was stirred for another 5 min before the glass bottle was heated at 105℃ in an electric oven for 12 h. After cooling down naturally, the product was harvested by several rinse-centrifugation cycles and fully dried at 60℃, then the black precipitates were sintered at 400℃ for 2 h under argon atmosphere to obtain the final composites of graphene@Fe_3O_4@SiO_2@NiO nanosheets.

2.2 Characterization

The obtained product was characterized by X-ray diffraction (XRD, PANalytical, Holland),

transmission electron microscopy (TEM, Philips Tecnai-12 transmission electron microscopy), X-Ray photoelectron spectroscopy (ESCALAB 250, Thermofisher Co), vibrating sample magnetometer (VSM). The electromagnetic parameters were analyzed using a HP8753D vector network analyzer. The measured samples were prepared by uniformly mixing 25 wt % of the sample with a paraffin matrix.

3. Results and discussion

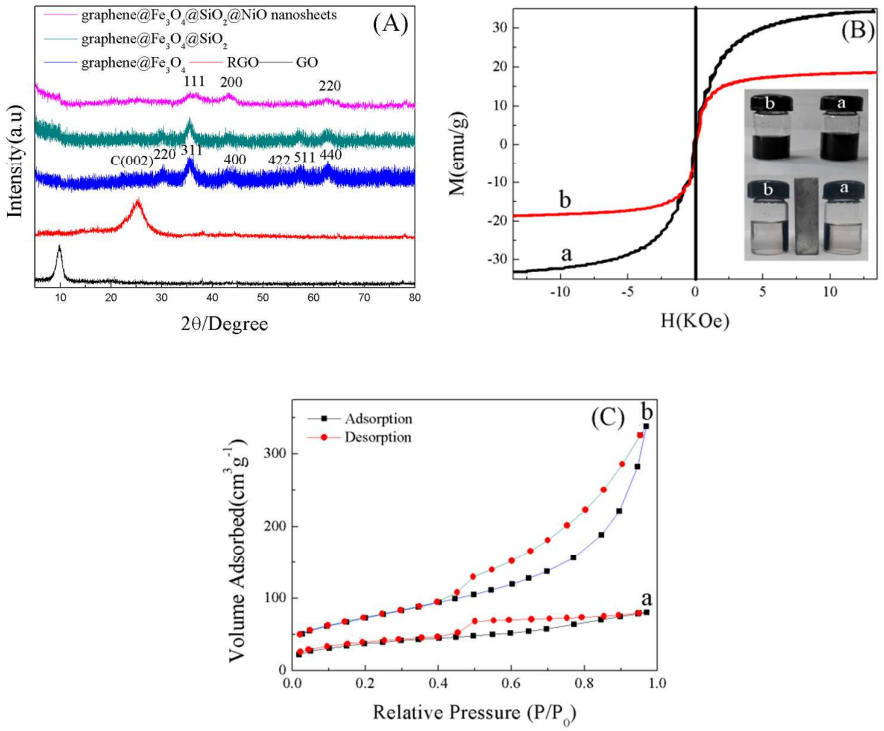

Fig. 1 XRD patterns of GO, RGO (reduced graphene oxide), graphene@Fe_3O_4, graphene@Fe_3O_4@SiO_2 and graphene@Fe_3O_4@SiO_2@NiO nanosheets (A), room-temperature magnetization curves (B), typical N_2 adsorption–desorption isotherms (C) of graphene@Fe_3O_4 (curve a) and graphene@Fe_3O_4@SiO_2@NiO nanosheets (curve b). (RGO was obtained by thermal expansion reduction of GO at 400℃ for 2 h under argon atmosphere.)

The phase and structures of the synthesized samples were characterized by XRD. Fig. 1 (A) shows the XRD patterns of GO, RGO obtained by thermal expansion reduction of GO at 400 ℃ for 2 h under argon atmosphere, graphene@Fe_3O_4 and graphene@Fe_3O_4@SiO_2@NiO nanosheets. For GO, the characteristic diffraction peak appears at around $2\theta = 9.8^{\circ}$ corresponding to the

interlayer spacing of 0.90 nm, which is due to the formation of the oxygen functionalities groups between the layers of GO. In the XRD pattern of RGO, the intense peak at 9.8° disappears and a broad band appears at 25.3° and its interlayer spacing is 0.34 nm. This shift in the d-spacing can be attributed to the successful reduction of GO and formation of graphitic structures. For graphene@Fe_3O_4, the detected diffraction peaks can be indexed in the cubic inverses spinel structure of Fe_3O_4 (JCPDS card, file No.19-0629), an additional small and broad diffraction peak around 23° corresponds to C(002) indicates the synthesis of graphene@Fe_3O_4 composites [22]. After reaction with TEOS, no characteristic peaks in related to other materials can be detected in graphene@Fe_3O_4@SiO_2, indicating the SiO_2 is amorphous. As for the graphene@Fe_3O_4@SiO_2@NiO nanosheets, the XRD pattern shows new characteristic diffraction peaks, which can be assigned to the cubic NiO structure (JCPDS, No. 71-1179).

The field-dependent magnetization for graphene@Fe_3O_4 and graphene@Fe_3O_4@SiO_2@NiO nanosheets was measured by a vibrating sample magnetometer at room temperature. As shown in Fig.1 (B), both graphene@Fe_3O_4 and graphene@Fe_3O_4@SiO_2@NiO nanosheets exhibit superaramagnetic behavior at room temperature with no coercivity and remanence. The value of M_s (saturation magnetization) decreases from 33.07 emu/g for graphene@Fe_3O_4 to 18.87 emu/g for graphene@Fe_3O_4@SiO_2@NiO nanosheets. This decrease in magnetism is attributed mainly to the decrease in weight ratio of Fe_3O_4 in the nanobybrids. When a magnet is placed beside a bottle filled with graphene@Fe_3O_4 and graphene@Fe_3O_4@SiO_2@NiO nanosheets dispersed in ethanol, the two nanohybrids quickly move along the magnetic field and accumulate near the magnet within a few minutes, leaving the solution transparent (inset of Fig.1 (B)).

The N_2 adsorption–desorption isotherms were measured to gain information about the specific

surface area of the graphene@Fe_3O_4 and graphene@Fe_3O_4@SiO_2@NiO nanosheets (Fig. 1(C)). This isotherm profile can be categorized as type IV with a small hysteresis loop observed at a relative pressure of 0.02–1.0. As calculated by Brunauer-Emmett-Teller (BET) method, graphene@Fe_3O_4@SiO_2@NiO nanosheets hierarchical structures gives rise to a BET area of 257.4 m^2g^{-1} and a relatively high pore volume of 0.551 cm^3g^{-1}, compared with 130.0 $m^2g^{-1}$and 0.093 cm^3g^{-1} for the graphene@Fe_3O_4.

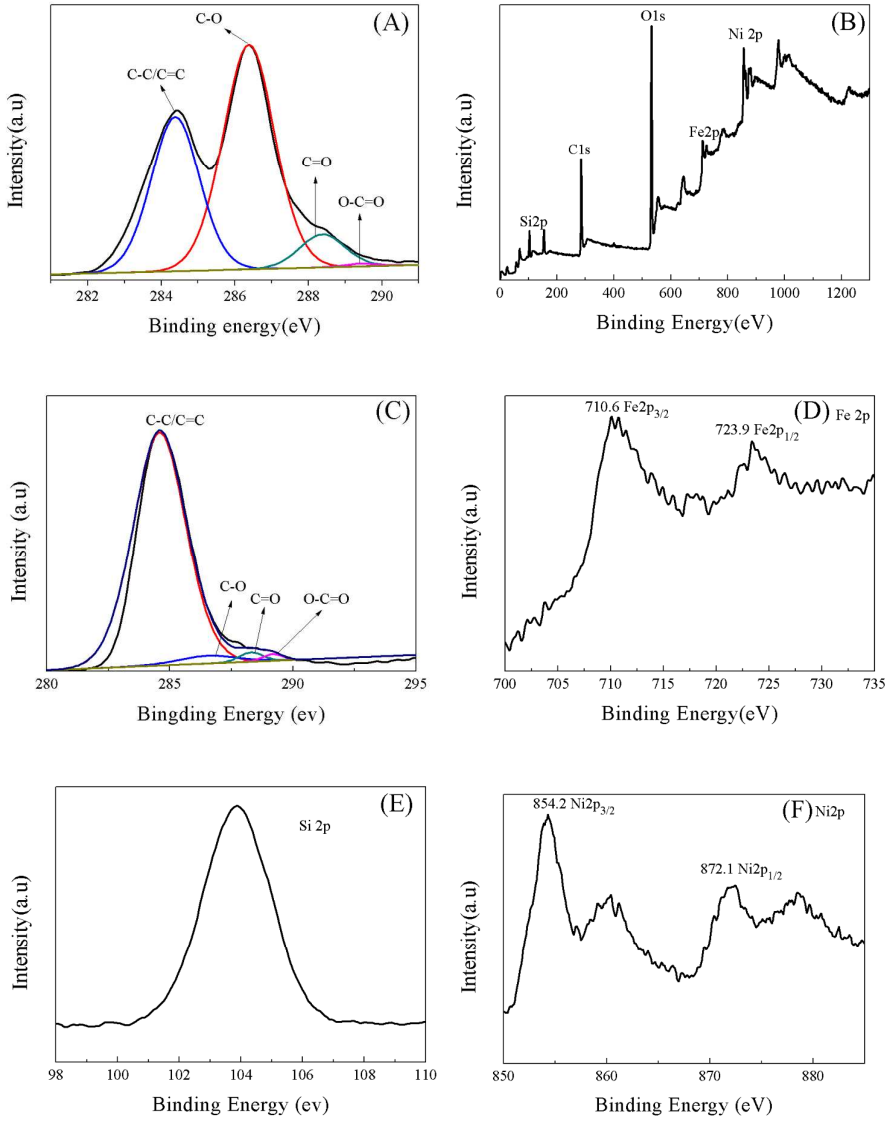

Fig.2 XPS spectra of Cls of GO (A), survey scan (B), C1s spectrum (C), Fe 2p spectrum (D) , Si 2p spectrum

(E), and Ni 2p spectrum (F) of graphene@Fe_3O_4@SiO_2@NiO nanosheets

Surface analysis of GO and the prepared graphene@Fe_3O_4@SiO_2@NiO nanosheets hierarchical nanostructures was carried out using XPS. Fig.2 (A) shows XPS spectra of Cls spectrum of GO. It clearly displays a considerable degree of oxidation with four components that correspond to carbon atoms in different functional groups: C-C/C=C (284.6 eV) in the aromatic rings, C-O (286.5 eV) of epoxy, C=O (288.3 eV) and O-C=O (289.1 eV) groups. The wide scan XPS spectrum (Fig.2 (B)) of graphene@Fe_3O_4@SiO_2@NiO nanosheets hierarchical structures shows photoelectron lines at a binding energy of 104.0, 284.6, 530.3, 711.3 and 852.4 eV attributed to Si2p, C1s, O1s, Fe2p and Ni2p, respectively. Compared with GO (Fig. 2(C)), the oxygen content of graphene@Fe_3O_4@SiO_2@NiO nanosheets decreases rapidly, and further suggest a remarkable reduction of GO. In Fig.2 (D), the binding energy peaks at 710.6 and 723.9 eV are corresponding to Fe $2p_{3/2}$ and Fe $2p_{1/2}$, suggesting the existence of Fe_3O_4 [24]. For Fig. 2(E), the peak at 104 ev confirms that the SiO_2 exists in the composites of graphene@Fe_3O_4@SiO_2@NiO nanosheets. In Fig.2 (F), the Ni $2p_{1/2}$ (872.1 eV) and Ni $2p_{3/2}$ (854.2 eV) peaks are assigned to the Ni(II) ions in NiO. The peak at 855.0 eV was ambiguous, and may be attributed to the Ni^{2+} species on the surface [25]. The energy difference between Ni $2p_{3/2}$ and $2p_{1/2}$ peaks is ~17.9 eV, indicating the well-defined symmetry of Ni(II) ion in oxide form [26].

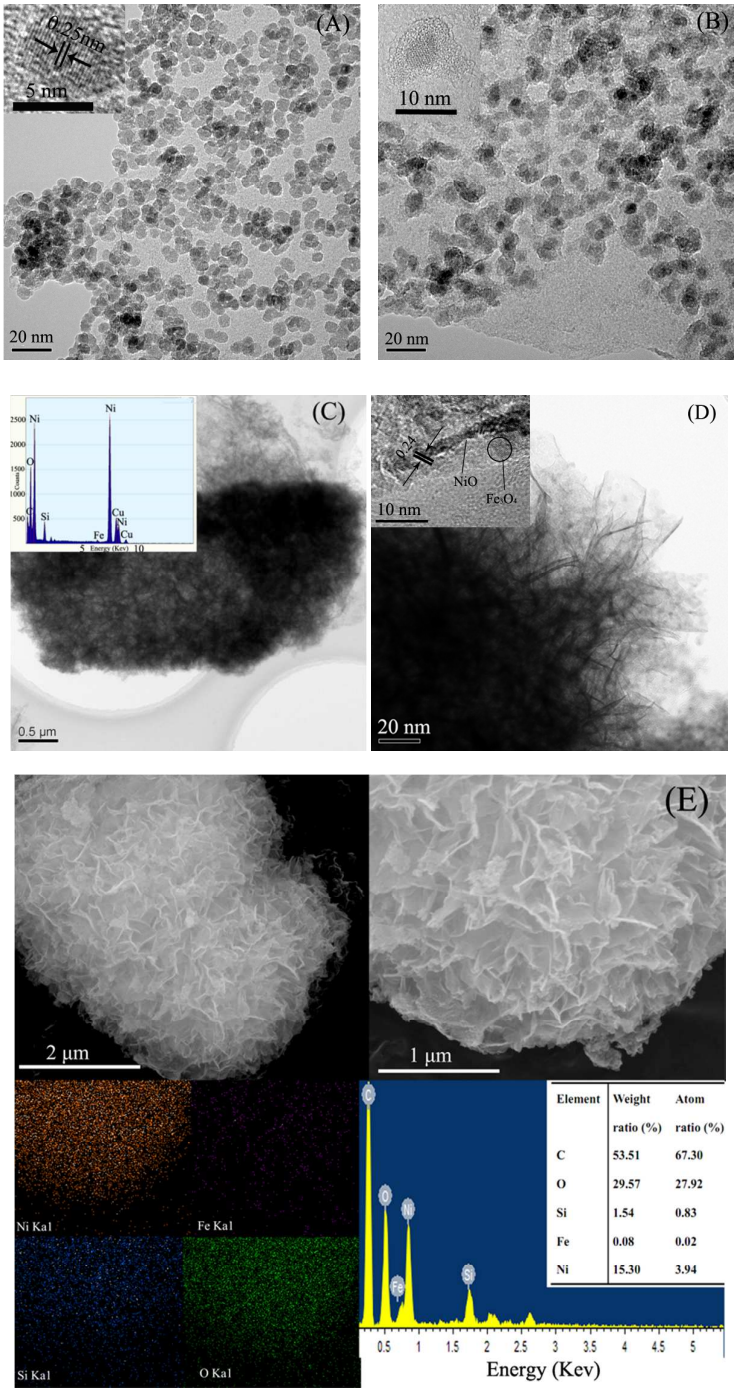

Fig.3 TEM images of graphene@Fe_3O_4 (A), graphene@Fe_3O_4@SiO_2 (B) and graphene@Fe_3O_4@SiO_2@NiO nanosheets composites (C and D), SEM images and corresponding EDX element Ni, Fe, Si and O maps of graphene@Fe_3O_4@SiO_2@NiO nanosheets. (Insets: The HRTEM images (A, B and D) and EDX pattern (C))

Fig.3 shows TEM image of graphene@Fe_3O_4 (A), graphene@Fe_3O_4@SiO_2 (B), graphene@Fe_3O_4@SiO_2@NiO nanosheets composites (C, D), SEM and EDS images of graphene@Fe_3O_4@SiO_2@NiO nanosheets and EDX element maps of Ni, Fe, Si and O. As shown in Fig.3 (A), the surfaces of graphene are densely covered by narrowly distributed Fe_3O_4 nanoparticles with an average size of 5 nm, and no big conglomeration of Fe_3O_4 nanoparticles or large vacancy on graphene is observed. The lattice fringe spacing (0.25 nm) displayed in HRTEM image (the inset in Fig.3 (A)) is well consistent with the lattice spacing of (311) planes of cubic magnetite. Fig.3 (B) shows the TEM image of graphene@Fe_3O_4@SiO_2, it is clear that Fe_3O_4@SiO_2 core-shell microstructures are formed on the surfaces of graphene, and SiO_2 layer is mainly coated on the surface of Fe_3O_4 nanoparticles. The HRTEM image (the inset in Fig.3 (B)) reveals that the average diameter of the Fe_3O_4@SiO_2 is around 10 nm and the thickness of SiO_2 is about 2.5 nm. Fig.3 (C) displays a typical TEM image of graphene@Fe_3O_4@SiO_2@NiO nanosheets composites. It is obvious that large two-dimensional structures can be observed under TEM microscope, and the corresponding energy-dispersive X-ray (EDX) image confirms the presence of Ni elements in the nanocomposites. The dark line in magnified TEM image (Fig.3 (D)) demarcates the edge of NiO nanosheets approximately oriented perpendicular to graphene@Fe_3O_4@SiO_2, and the corresponding HRTEM image (the inset in Fig.3 (D)) reveals lattice fringes with a distance of 0.24 nm corresponding to (111) planes of cubic crystalline NiO. As shown in Fig.3 (E), SEM images of graphene@Fe_3O_4@SiO_2@NiO nanosheets are consistent with the above TEM analysis and the NiO nanosheets are mostly grown upright with a random orientation on top of the graphene@Fe_3O_4@SiO_2 support.

Moreover, EDX (energy dispersive X-ray) mapping results (elements distribution of Ni, Fe, Si and O) further confirm that NiO nanosheets are grown on the surface of graphene@Fe_3O_4@SiO_2 and the contents of C, O, Si, Fe and Ni are 67.3%, 27.92%, 0.83%, 0.02% and 3.94%, respectively.

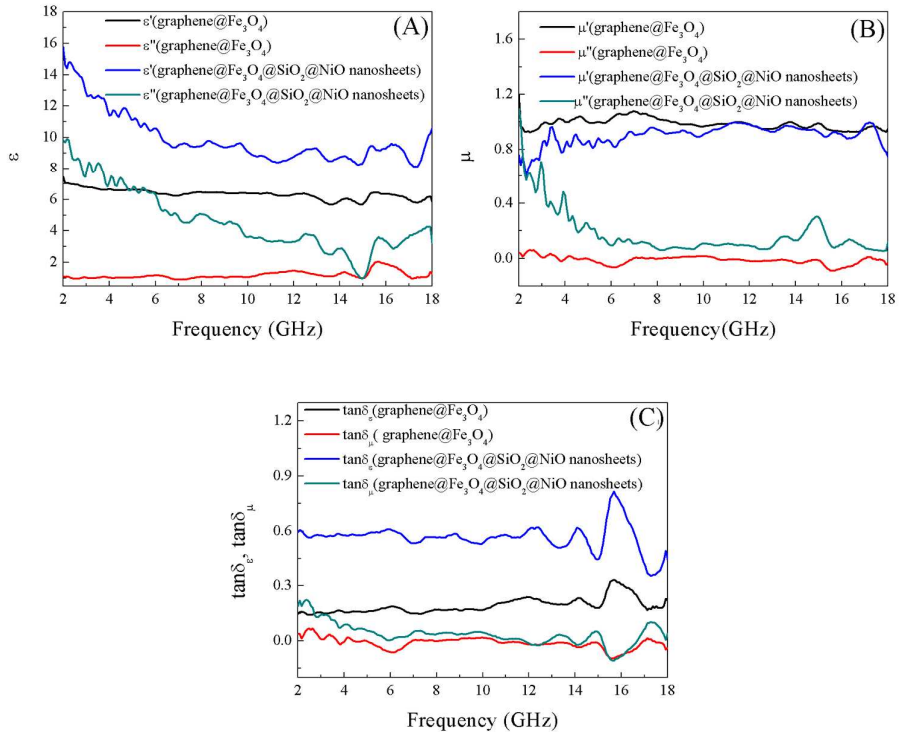

Fig. 4 Complex permittivity (A), permeability (B), dielectric loss tangent and magnetic loss tangent (C) from 2 to 18 GHz for graphene@Fe_3O_4 and graphene@Fe_3O_4@SiO_2@NiO nanosheets composites with 25 wt.%.

The microwave absorption property of materials is generally determined by the complex relative permittivity and permeability as well as the tangent loss of both dielectric tangent loss ($\tan\delta_\varepsilon=\varepsilon''/\varepsilon'$) and magnetic tangent loss ($\tan\delta_\mu=\mu''/\mu'$). Fig. 4 (A) presents the real part (ε') and imaginary (ε") of the complex permittivity of graphene@Fe_3O_4, graphene@Fe_3O_4@SiO_2 and

graphene@Fe_3O_4@SiO_2@NiO nanosheets composites. For the graphene@Fe_3O_4 composites, the ε' value is in the range of 7.1-6.4 and ε" is in the range of 1.1-1.9. When the graphene@Fe_3O_4@SiO_2@NiO nanosheets hierarchical structures are fabricated, the ε' value increases to a range of 15.6-8.3 and ε" value floats in the range of 9.8-1.2. It can be seen that both ε' and ε" values of graphene@Fe_3O_4@SiO_2@NiO nanosheets composite are higher than those of graphene@Fe_3O_4. The real part (ε') is mainly associated with the amount of polarization occurring in the material, and the imaginary part (ε") is related to the dissipation of energy. The dielectric performance of the material depends on ionic, electronic, orientational (arising due to the presence of bound charges) and space charge polarization (due to the heterogeneity in the system). In a heterogeneous system, the accumulation of virtual charges at the interface of two media having different dielectric constants leads to interfacial polarization, which is known as Maxwell-Wagner polarization [27]. Here, the higher ε' for graphene@Fe_3O_4@SiO_2@NiO nanosheets is mainly arising from the introduction of NiO since it exhibits an intrinsic property of NiO (the static dielectric constant of bulk NiO is 10.31 or 11.75.), and ε" for graphene@Fe_3O_4@SiO_2@NiO nanosheets may be ascribe to the enhanced polarization induced by the multi-interfaces and triple junctions (graphene@Fe_3O_4, Fe_3O_4@SiO_2, SiO_2@NiO nanosheets) as well as associated loss mechanism.

Fig. 4 (B) shows the real part (μ') and imaginary part (μ") of the complex permeability of graphene@Fe_3O_4 and graphene@Fe_3O_4@SiO_2@NiO nanosheets composites. Compared with graphene@Fe_3O_4, the μ' value of graphene@Fe_3O_4@SiO_2@NiO nanosheets is lower in the range of 2-11 GHz and exhibits low difference in range of 11-18 GHz, while the μ" is higher

through the whole frequency range. Higher values of μ" for graphene@Fe_3O_4@SiO_2@NiO nanosheets composites can be attributed to the magnetic losses in NiO nanosheets.

Fig. 4(C) shows the dielectric tangents tanδ_ε loss and magnetic tangent loss of tanδ_μ of graphene@Fe_3O_4 and graphene@Fe_3O_4@SiO_2@NiO nanosheets composites. It is clear that graphene@Fe_3O_4@SiO_2@NiO nanosheets composites possess a far higher dielectric tangent loss than graphene@Fe_3O_4. The enhanced dielectric loss could stem from the enhanced interfacial polarization relaxation in graphene@Fe_3O_4@SiO_2@NiO nanosheets composites. For the magnetic tangent loss, the value of graphene@Fe_3O_4@SiO_2@NiO nanosheets is slightly greater than that of graphene@Fe_3O_4 composites. It indicates that graphene@Fe_3O_4@SiO_2@NiO nanosheets composites may possess better microwave absorption properties. In addition, it is worth noting that the dielectric tangent loss of the two composites is greater than the magnetic tangent loss, suggesting that the dielectric loss makes a major contribution to the electromagnetic loss.

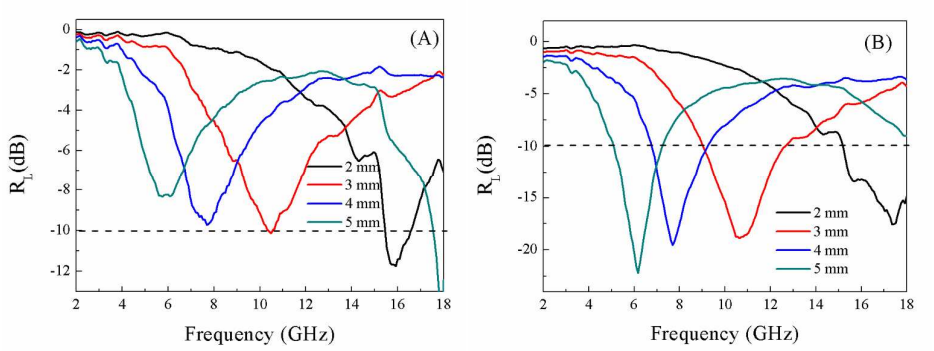

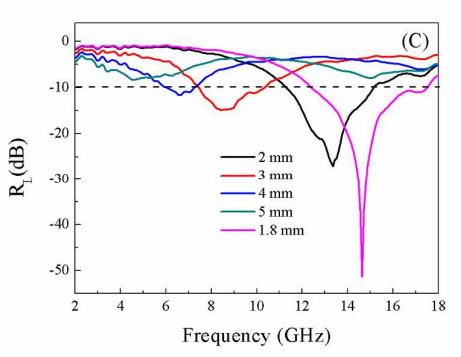

Fig.5 The calculated reflection losses for graphene@Fe_3O_4 (A), graphene@Fe_3O_4@SiO_2 (B) and graphene@Fe_3O_4@SiO_2@NiO nanosheets (C) paraffin wax composites with different thicknesses in the frequency range of 2-18 GHz

To further study the microwave absorption properties, the reflection losses (R_L) of the NiO@SiO_2@graphene and SiO_2@graphene composites can be evaluated by

$$R_L(\mathrm{dB}) = 20\left|\log\frac{Z_{in}-1}{Z_{in}+1}\right| \quad (1)$$

While the normalized input impedance (Z_{in}) was calculated by

$$Z_{in} = \sqrt{\frac{\mu_r}{\varepsilon_r}}\tanh\left(\mathrm{j}\frac{2\pi fd}{c}\sqrt{\mu_r\varepsilon_r}\right) \quad (2)$$

where f is the microwave frequency, d is the thickness of the absorb layer, c is the velocity of electromagnetic wave in vacuum, and ε_r and μ_r are the complex relative permittivity and permeability, respectively. The calculated reflection loss (R_L) curves of the graphene@Fe_3O_4 and graphene@Fe_3O_4@SiO_2@NiO nanosheets composites with different thickness are shown in Figure 5. In the investigated region, graphene@Fe_3O_4@SiO_2@NiO nanosheets composites exhibit significantly enhanced microwave absorption compared with graphene@Fe_3O_4. As shown in Fig.5 (A), graphene@Fe_3O_4 composites exhibit the maximum R_L of -11.7 dB at the optimal sample thickness of 2.0 mm and the R_L values under -10 dB absorption frequency range from 15.4 to 16.5 GHz. After coating SiO_2 on Fe_3O_4 surfaces, the maximum R_L increases to -22.1 dB and the R_L

values under -10 dB is 2.2 GHz (Fig.5 (B)). When NiO nanosheets are fabricated on the surfaces of graphene@Fe_3O_4@SiO_2 and form the hierarchical structures, the maximum R_L value increases to -51.5 dB at 14.6 GHz with a thickness of only 1.8 mm and a bandwidth corresponding to the reflection loss below -10 dB is 5.1 GHz (from 12.4 to 17.5 GHz) (Fig.5(B)). It is clear that graphene@Fe_3O_4@SiO_2@NiO nanosheets composites display enhanced microwave absorption properties in terms of both the maximum R_L values and the absorption bandwidths. In addition, the effect of wt% incorporation of absorbers on the microwave absorption of measured samples was also investigated. Fig.6 shows the theoretical R_L of graphene@Fe_3O_4@SiO_2@NiO nanosheets-wax composites with different loadings in the range of 2-18 GHz at a thickness of 1.8 mm. It is clearly that 25 wt% graphene@Fe_3O_4@SiO_2@NiO nanosheets-wax composites show the best microwave absorption performance, and the suitable loadings of absorbers is 25 wt%.

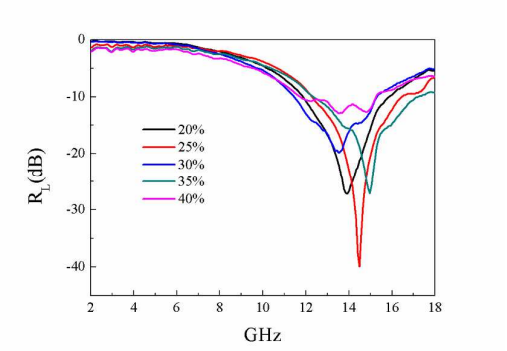

Fig. 6 the reflection loss of the graphene@Fe_3O_4@SiO_2@NiO nanosheets-wax composites with different loadings at a thickness of 1.8 mm.

The enhanced absorption properties of graphene@Fe_3O_4@SiO_2@NiO nanosheets hierarchical structures can be explained by the following facts. Firstly, the multi-interfaces and triple junctions (graphene@Fe_3O_4, Fe_3O_4@SiO_2, SiO_2@NiO) are advantageous for electromagnetic attenuation due to the existing interfacial polarization [28]. Secondly, the NiO nanosheets and the void space

existing between Fe_3O_4 and NiO nanosheets result in relatively large specific surfaces areas and high porosities, providing more active sites for reflection and scattering of electromagnetic wave [29]. Finally, the void space between Fe_3O_4 and NiO nanoflower can effectively interrupt the spread of electromagnetic wave and generate dissipation due to the existing impendence difference and enhanced the microwave absorption properties [30].

4. Conclusion

In summary, hierarchical structures of graphene@Fe_3O_4@SiO_2@NiO nanosheets were prepared by combining the versatile sol-gel process with hydrothermal reaction. When evaluated as microwave absorbers, the hierarchical structures exhibit enhanced microwave absorption properties in terms of both the maximum reflection loss value and the absorption bandwidth. The maximum reflection loss of graphene@Fe_3O_4@SiO_2@NiO nanosheets is -51.5 dB at 14.6 GHz and the absorption bandwidth with a reflection loss below -10 dB ranges from 12.4 to 17.5 GHz with a thickness of only 1.8 mm. Thus, it is believed that such hierarchical structures will find their wide applications in microwave absorbing area.

References

[1] G. B. Sun, B.X. Dong, M.H. Cao, B.Q. Wei, C.W. Hu, Chem. Mater., 2011,23, 1578.

[2] C. L. Zhu, J. Phy. Chem. C, 2010, 114, 16229.

[3] H. S. Pan, X. Q. Cheng, C. H. Zhang, C. H. Gong, L. G. Yu, J. W. Zhang, Z. J. Zhang, Appl. Phys. Lett., 2013,102, 012410.

[4] L. C. Li, C. Xiang, X. X. Liang, B. Hao, Synth. Met., 2010, 160, 28.

[5] J. W. Liu, R. C. Che, H. J. Chen, F. Zhang, F. Xia, Q. S. Wu, M. Wang, Small, 2012, 8, 1214.

[6] P. Xu, X. J. Han, C. Wang, D. H. Zhou, Z. H. Lv, A. H. Wen, X. H. Wang, B. Zhang, J. Phys. Chem. B, 2008, 112, 10443.

[7] R. C. Che, L. M. Peng, X. F. Duan, Q. Chen, X. L. Liang, Adv. Mater., 2004, 16, 401.

[8] M. S. Cao, J. Yang, W. L. Song, D. Q. Zhang, B. Wen, H. B. Jin, Z. L. Hou, J. Yuan, ACS Appl.

Mater. Interfaces, 2012, 4, 6949.

[9] H. J. Wu, L. D. Liu, Y. M. Wang, S. G. Guo, Z. G. Shen, J. Ally. Com., 2012, 525, 82.

[10] P. Saini, V. Choudhary, B. P. Singh, R. B. Mathur, S. K. Dhawan, Mater. Chem. Phys., 2009, 113, 919.

[11] K. S. Novoselov, A.K. Geim, S.V. Morozov, D. Jiang, Y. Zhang, S.V. Dubonos, I.V. Grigorieva, A. Fiesov, Science, 2004, 306,666.

[12] C. Wang, X. J. Han,P. Xu, X.L. Zhang,Y.C. Du, S.R. Hu, J.Y. Wang, X.H. Wang, Appl. Phys. Lett. 98 (2011) 072906.

[13] T. S. Wang, Z. H. Liu, M. M. Lu, B. Wen, Q.Y. Ouyang, Y. J. Chen, C. L. Zhu, P. Gao, C. Y. Li, M. S. Cao, L.H. Qi, J. Appl. Phys. 113 (2013) 024314

[14] X. Sun, J. P. He, G. X. Li, J. Tang, T. Wang, Y. X. Guo, H. R. Xue, J. Mater. Chem. C, 2013, 1 765-777.

[15] H. L. Xu, H. Bi, R. B Yang, Appl. Phys., 2012, 111,07A522.

[16] Y. L. Ren, H.Y. Wu, M. M. Lu, Y.J. Chen, C. L. Zhu, P. Gao, M. S. Cao, C. Y. Li, Q.Y. Ouyang, Appl. Mater. Interfaces, 2012, 4, 6436.

[17] D.Z. Chen, G.S. Wang, S. He, J. Liu, L. Guo, M. S. Cao, J. Mater. Chem. A ,2013, 1, 5996.

[18] H. F. Li, Y. H. Huang, G. B. Sun, X. D. Yan, Y. Yang, J. Wang, Y. Zhang, J. Phys. Chem. C, 2010, 114, 10088.

[19] J. W. Liu, J. J. Xu, R. C. Che, H. J. Chen, Z. W. Liu, F. Xia, J. Mater. Chem., 2012, 22, 9277.

[20] D. B. Wang, C. X. Song, Z. S. Hu, X. Fu, J. Phys. Chem. B, 2005, 109, 1125.

[21] J. P. Zhao, S. F. Pei, W. C. Ren, L. B. Gao, H. M. Cheng. ACS Nano, 2010, 4, 5245.

[22] H. K. He, C. Gao, ACS Appl. Mater. Interfaces, 2010, 2 (11), 3201.

[23] T. Zhu, H. B. Wu, Y.B. Wang, R. Xu, W. X. Lou. Adv Energy Mater 2012, 2(12), 1497.

[24] C. K. Lo, D. Xiao, M. M. F. Choi, J. Mater. Chem., 2007, 17, 2418.

[25] M. Tomellini, J. Electron Spectrosc. Relat. Phenom., 1992,58, 75.

[26]S. W. Zhang, J. X. Li, T. Wen, J. Z. Xu, X.K. Wang, RSC Adv., 2013, 3, 2754.

[27]J. Zhu, H. Gu, Z. Luo, N. Haldolaarachige, D. P. Young, S.Wei, Z. Guo, Langmuir, 2012, 28, 10246.

[28] G.B. Sun, B.X. Dong, M.H. Cao, B.Q. Wei, C.W. Hu, Chem. Mater., 2011, 23,1587.

[29] H.F. Li, Y.H. Huang, G.B. Yan, X.Q. Yan, Y. Yang, Wang J, J. Phys. Chem. C, 2010, 114, 10088.

[30] Y. Qin, R.C. Che, C.Y. Liang, J. Zhang, Z.W. Wen, J. Mater. Chem., 2011, 21, 3960.

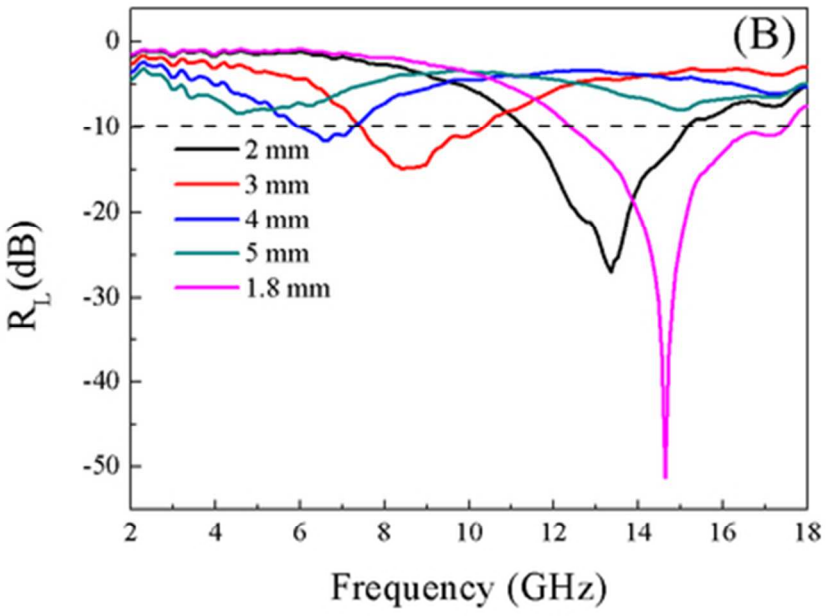

Graphical Abstract
20x14mm (600 x 600 DPI)